AIAA 2002-2997

COMPUTATIONAL ANALYSIS OF TOWED BALLUTE INTERACTIONS

Peter A. Gnoffo†
p.a.gnoffo@larc.nasa.gov
NASA Langley Research Center

Brian P. Anderson‡
b.p.anderson@larc.nasa.gov
GWU – JIAFS

Hampton, VA 23681-0001

Abstract

A ballute (balloon-parachute) is an inflatable, aerodynamic drag device for application to planetary entry vehicles. Ballutes may be directly attached to a vehicle, increasing its cross-sectional area upon inflation, or towed behind the vehicle as a semi-independent device that can be quickly cut free when the requisite change in velocity is achieved. The aerothermodynamics of spherical and toroidal towed ballutes are considered in the present study. A limiting case of zero towline length (clamped system) is also considered. A toroidal system can be designed (ignoring influence of the tethers) such that all flow processed by the bow shock of the towing spacecraft passes through the hole in the toroid. For a spherical ballute, towline length is a critical parameter that affects aeroheating on the ballute being towed through the spacecraft wake. In both cases, complex and often unsteady interactions ensue in which the spacecraft and its wake resemble an aero spike situated in front of the ballute. The strength of the interactions depends upon system geometry and Reynolds number. We show how interactions may envelope the base of the towing spacecraft or impinge on the ballute surface with adverse consequences to its thermal protection system. Geometric constraints to minimize or eliminate such adverse interactions are discussed. The towed, toroidal system and the clamped, spherical system show greatest potential for a baseline design approach.

Nomenclature

D	diameter, m
L	separation distance, m
M	Mach number
$\mathcal{M}$	molecular weight, kg/kmole
q_w	wall heat transfer rate, W/cm^2
r	radial distance, m
R_C	toroid cross-section radius, m
R_I	toroid inner (hole) radius, m
Re	$\rho_\infty V_\infty L / \mu_\infty$, Reynolds number
T	temperature, K
V	velocity, km/s
x, y, z	Cartesian coordinates
χ_i	mole fraction of species i
ρ	density, kg/m^3

Subscripts

i	species index
w	wall surface conditions
∞	freestream conditions

† Senior Research Engineer, Aerothermodynamics Branch, Associate Fellow AIAA
‡ Graduate Student, Student Member AIAA

Introduction

Large, inflatable ballutes (balloon-parachutes) have been proposed[1,2] as hypersonic decelerators for planetary aerocapture applications. Ballutes may be attached to a vehicle, increasing its cross-sectional area upon inflation, or towed behind the vehicle as a semi-independent device that can be quickly cut free when the requisite change in velocity is achieved. Aeroheating on spherical and toroidal ballutes has been documented for the limiting, most benign case that ignores interactions from the wake of the towing spacecraft[3]. This paper presents a status of towed-ballute system simulations including axisymmetric interactions based on continuum analyses. Future work will move beyond axisymmetric and continuum limitations, focusing on the most promising systems identified in this initial scoping effort. Effects of interactions between the towlines and the spacecraft-ballute system are also deferred for a subsequent study.

Numerical simulations are conducted with the Langley Aerothermodynamic Upwind Relaxation Algorithm (LAURA[4]). Physical models in LAURA have been updated[3] to include chemical species expected in the shock layer of ballutes entering the atmospheres of Venus, Saturn, Titan, and Neptune – in addition to the models for Mars and Earth already present. However, most of the simulations presented here utilize a perfect-gas approximation to quickly scope relative effects of spacecraft – ballute separation distance.

The first system considered is a spacecraft – toroidal ballute for the Titan Organics Explorer mission. In this case, separation distance is constrained by a requirement that the wake of the spacecraft pass through the toroid with minimal interaction to the ballute surface. Given this constraint, effects of Reynolds number for a fixed towline length are studied to scope interaction effects on aeroheating on both the ballute and base of the towing spacecraft. Important considerations of interactions associated with angle of attack have not yet been addressed for such a system. Limited results for angle of attack on the toroidal system without interactions from the spacecraft are introduced.

The second system considered is a spacecraft – spherical ballute at identical freestream conditions to the toroidal system. Here, aeroheating on the spherical ballute is strongly influenced by separation distance. These environments are studied as a function of separation distance for a single trajectory point. Effects of varying Reynolds number for a single separation length are also studied. Finally, a special case of zero separation is presented (the base of the spacecraft is contained within the spherical ballute) that shows a relatively benign interaction environment.

Configurations

The towed, spherical ballute system is shown in Fig. 1 and the towed, toroidal ballute system is shown in Fig. 2. A Viking shaped towing spacecraft six meters in diameter is utilized in all simulations of interacting flows presented herein. System geometric parameters are indicated on each figure. The spherical system in Fig. 1 has a towline length, L, equal to 100 m and ballute diameter, D, equal to 70m. The toroidal system in Fig. 2 has a towline length, L, equal to 28.46 m, toroid diameter, D, equal to 52 m, cross-sectional radius, R_C, equal to 6.5 m, and inner (hole) radius, R_I, equal to 19.5 m. (Note that $R_I = D/2 - R_C$). Pressure contour lines are included to qualitatively define the nature and extent of the interaction of the spacecraft wake with the shock layer surrounding the ballute. These interactions will be discussed in later

sections. Figs. 1 and 2 show the entire symmetry plane; only the half symmetry plane to the axis will be shown in subsequent figures of axisymmetric flow simulations.

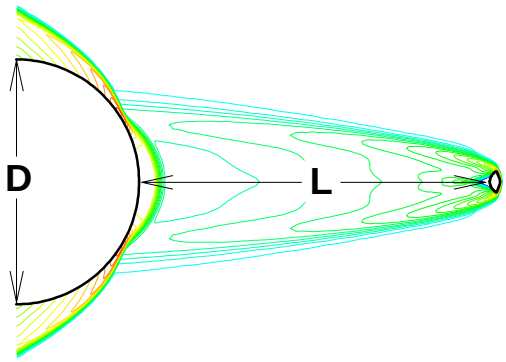

Fig. 1: Towed, spherical ballute system symmetry plane.

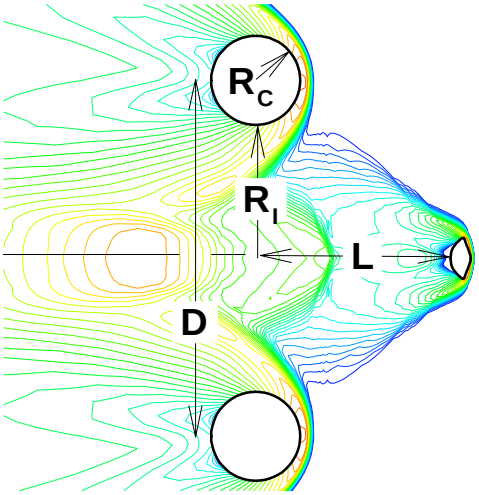

Fig. 2: Towed, toroidal ballute system symmetry plane.

Non-Interacting Simulations

A brief review of results from Reference 3 is presented in Table 1 for drag coefficient and stagnation point surface temperature on spherical and toroidal ballutes without interaction from the towing spacecraft wake. Table 1 includes trajectory point data, ballute geometric parameters, and freestream atmospheric constituents. The toroid simulations assume incoming flow aligned with the generatrix. All simulations were obtained assuming laminar flow in thermochemical nonequilibrium. A surface emissivity of 0.9 is assumed. A conservative, "super catalytic" surface approximation is applied (tending to produce higher heating rates than a finite- or non-catalytic boundary condition) in which species mole fractions at the surface are returned to their freestream values.

For a typical mission considered in Table 1 a ballute must survive an aeropass (remain inflated) for approximately ten minutes. Laminates of Kapton film with polybenzoxazole (PBO) are believed to combine the needed tensile strength and temperature limits (up to 770 K) required in this application[1]. Calculated environments in Table 1 show peak temperatures in the range of 677 K to 865 K. Further reductions in aeroheating may be achieved with larger ballutes or advanced materials may increase the temperature limits. For now, systems defined in Table 1 serve as credible placeholders for a fixed geometry ignoring interaction effects. (The non-interacting result is reasonable for the toroid if the hole is sufficiently larger than the spacecraft wake and interactions from relatively thin towlines can be ignored. The non-interacting result for a towed sphere would only be valid for exceptionally long towlines for which the spacecraft wake is fully dissipated.)

Table 1 – Non-Interacting Ballute Simulations

Mission	Venus Sample Return	Mars Microsat	Saturn Ring Observer	Titan Organics Explorer	Neptune Orbiter
Atmosphere, $\chi_{i,\infty}$	CO_2 = .965 N_2 = .035	CO_2 = .953 N_2 = .027 Ar = .016 O_2 = .004	H_2 = .963 He = .037	N_2 = .983 CH_4 = .017	H_2 = .80 He = .19 CH_4 = .01
Sphere, D, m	135.	12.	120.	48.	100.
V_∞, km/s	10.6	5.54	24.1	8.53	26.7
ρ_∞, kg/m^3	2.2 10^{-7}	1. 10^{-6}	3.1 10^{-8}	3.0 10^{-7}	1.5 10^{-8}
C_D	0.913	0.99	0.98	0.981	1.05
$\dot{q}_{max}$, W/cm^2	1.07	1.82	2.72	1.93	2.60
T_{max}, K	677.	774.	855.	785.	845.
Toroid, m Ring D / X-sec D	150. / 30.	15. / 3.	120. / 30.	52. / 13.	100. / 25.
V_∞, km/s	10.6	5.49	23.9	8.55	26.8
ρ_∞, kg/m^3	1.6 10^{-7}	7.1 10^{-7}	2.3 10^{-8}	1.9 10^{-7}	8.2 10^{-9}
C_D	1.31	1.45	1.38	1.39	1.51
$\dot{q}_{max}$, W/cm^2	1.31	1.91	2.85	2.05	2.84
T_{max}, K	712.	783.	865.	796.	864.

Recent work presented herein will explore effects of interactions from the spacecraft wake on aeroheating as a function of geometry and Reynolds number. Effects of toroidal geometry variations and gas chemistry model for the non-interacting case are discussed below.

Toroid Geometry Issues

Even without influence of the towing spacecraft wake, flow through the core of the toroidal ballute exhibits strong self-interaction effects associated with the convergence of the bow shocks. We review these interactions to set the stage for the two-body interactions that follow.

It is intuitively obvious that as the radius of the hole, R_I, in the toroid decreases (for fixed cross-sectional radius, R_C) the flow through the hole will choke. This effect is demonstrated in Figs. 3 and 4 for flow of air modeled as a perfect gas at V_∞ = 5 km/s, $\rho_\infty = 10^{-3}$ kg/m^3, and T_∞ = 200 K. (M = 17.6, Re = 377,000/m) through toroids with constant R_C = 5.0 m and R_I equal to 40.0 m (R_C/R_I = 0.125, Fig.3), and 10.0 m (R_C/R_I = 0.5, Fig. 4). Each figure presents color contours of pressure in a symmetry plane (y = 0.) extending from the axis of symmetry (x = y = 0.) to the inflow boundary ahead of the bow shock. Only the upper cross-sectional cut of the toroid is shown. Flow is from right to left, in the negative z direction. The freestream inflow boundary appears as a red line. The bow shock is the abrupt boundary between the high-pressure (cyan and red) regions and the low, freestream pressure (deep blue).

Grid adaptation parameters in LAURA used a cell Reynolds number of order 1, 120 circumferential cells and 64 cells from the body to the farfield boundary or toroid axis. Grid topology at the axis, particularly in Fig. 4, is highly skewed relative to the captured shock. A multiblock topology would be better suited to resolve

this structure. The current grid is considered adequate to demonstrate these qualitative trends based on grid refinement studies of related problems discussed later.

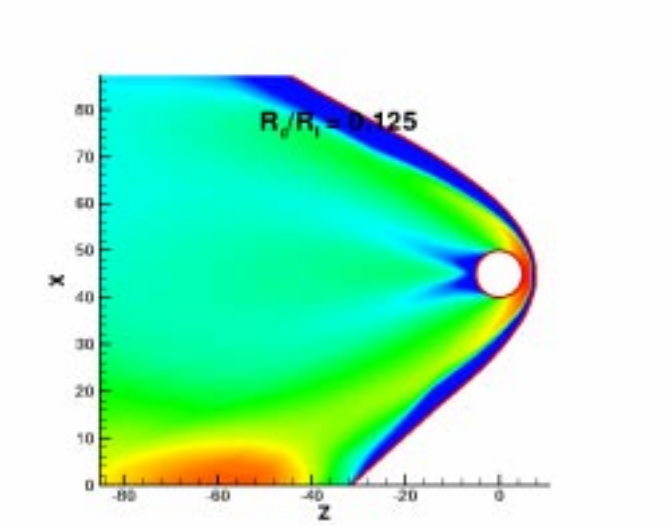

Figure 3: Pressure contours in the symmetry plane over toroid with $R_C/R_I = 0.125$.

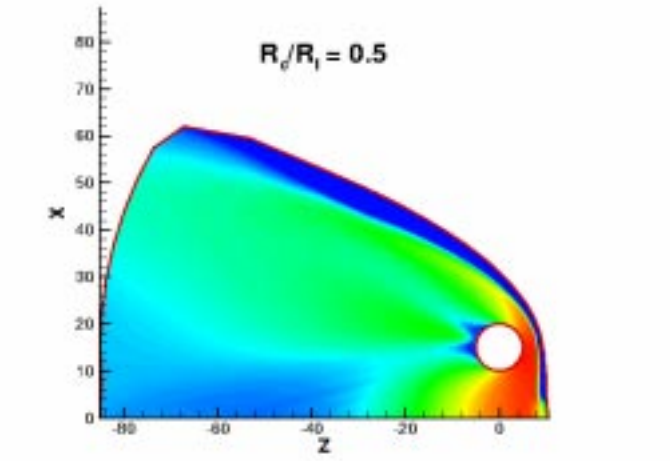

Figure 4: Pressure contours in the symmetry plane over toroid with $R_C/R_I = 0.5$.

Core flow in the toroid is also strongly influenced by gas chemistry. The gas chemistry for the Titan Organics Explorer in Table 1 is modeled as a perfect gas with $\gamma = 1.4$ in Fig. 5 and as a gas in thermochemical nonequilibrium in Fig. 6. The additional thermal and chemical degrees of freedom (lower effective γ) promote a smaller shock standoff distance and converging shocks further back on the axis. The net effect is that larger effective γ enhances stronger self-interaction and larger Mach disc in the core flow. Smaller effective γ promotes more complete supersonic flow through the core.

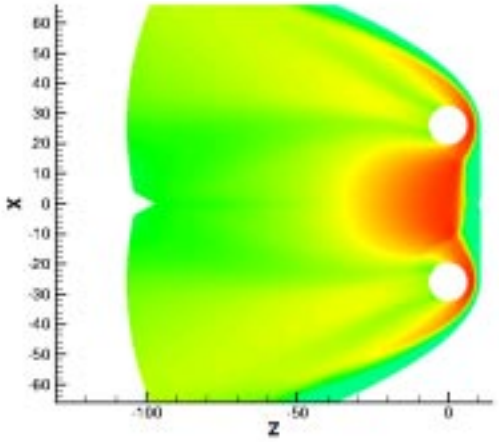

Figure 5: Pressure contours in the symmetry plane over toroid at two degrees angle of attack using perfect-gas model with γ=1.4.

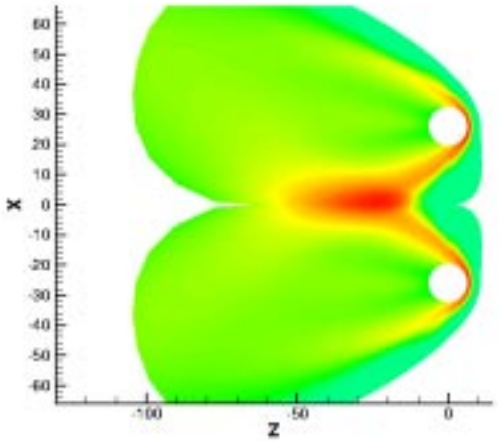

Figure 6: Pressure contours in the symmetry plane over toroid at two degrees angle of attack using Titan atmospheric model in thermochemical nonequilibrium.

One might expect a weaker interaction with the towing spacecraft using the thermochemical nonequilibrium model because the zone of subsonic flow is greatly diminished. This effect can be approximated in a perfect gas model by reducing the effective γ and the mixture molecular weight as discussed in the next section on interacting flows.

Results in Figs. 5 and 6 were computed at two degrees angle of attack. Both cases were aerodynamically stable relative to the center of the toroid at x=0 and z=0. Aerodynamic stability, including effects of interactions with the towing spacecraft wake in three dimensions, has not yet been evaluated.

Spacecraft – Toroid Interactions

The non-interacting flow at M_∞ = 26.3 between a Viking-shaped spacecraft and a toroidal ballute for conditions defined in Table 1 (Titan Organics Explorer) is shown in Fig. 7. The towing spacecraft has a 3.0 m maximum radius. Effects of towlines are not included. Temperature contours are featured. A perfect gas with effective γ=1.2 and $\mathcal{M}$ = 18.9 is applied to save computational time; however, it is evident that the shock shape and Mach disk in the hole of the toroidal ballute is qualitatively similar to that seen in Fig. 6 using the more complete thermochemical model. The boundary between the spacecraft grid domain and the ballute grid domain is evident in Fig. 7 at z=10 where the wake of the spacecraft abruptly terminates. A simple extrapolation boundary condition was used to terminate the spacecraft flowfield whereas constant inflow conditions were used to feed the ballute flowfield.

The value of R_C/R_I is 0.333 for this case. If γ was equal to 1.4 then a larger Mach disc in the core (something between Fig. 3 and Fig. 4) would be expected. However, the lower γ (and higher Mach number) cause the converging shocks to interact further back on the axis.

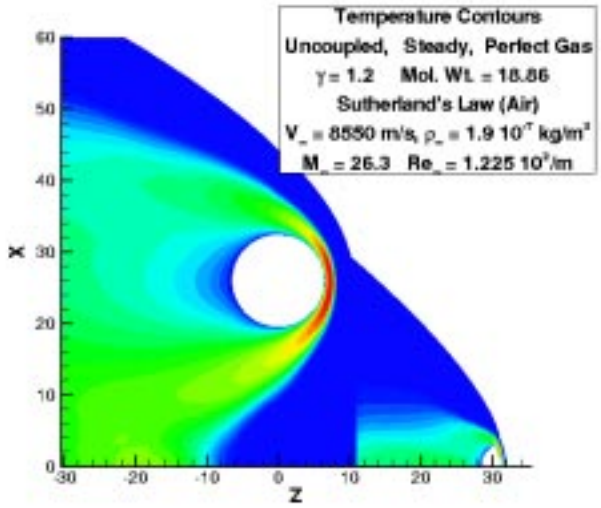

Figure 7: Temperature distribution in plane of symmetry for non-interacting spacecraft-ballute system with perfect-gas model using effective γ=1.2 for Titan Organics Explorer.

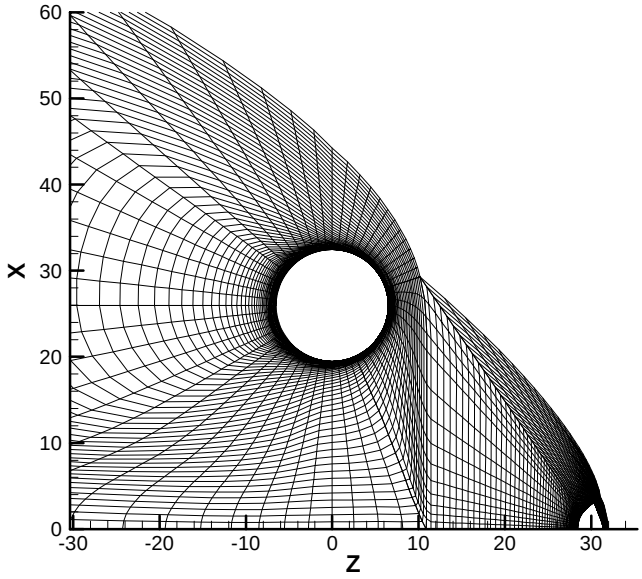

Figure 8: Mesh for spacecraft – toroid interaction study.

The toroid domain in Fig. 8 is resolved with 60 circumferential cells and

64 cells normal to the body, with cell Reynolds number of order 1 at the body. The spacecraft domain has the same grid metrics. Grid quality in the near vicinity of the toroid and spacecraft is considered adequate for good resolution of heat transfer, based on experience with related simulations. Grid quality along the spacecraft wake is relatively coarse and the solution of the wake interaction region is probably not grid converged. Of greater concern is that Knudsen numbers in the wake feeding the interaction region are of order 1 or higher based on local densities and wake-core diameter. Ongoing work will address these deficiencies; for now the interaction trends that follow should be considered qualitative.

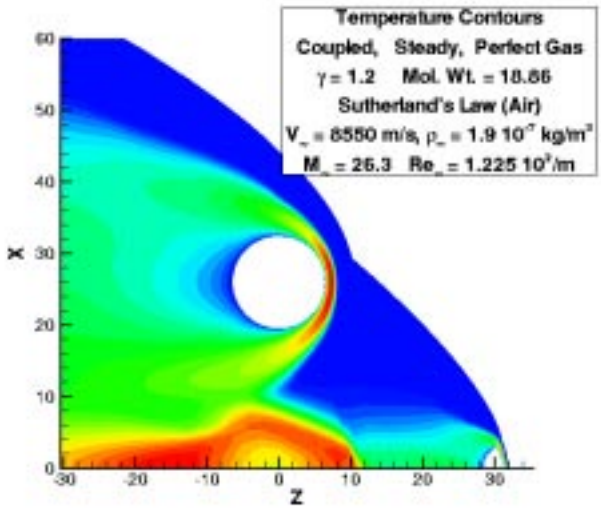

Figure 9: Temperature distribution in plane of symmetry for interacting spacecraft-ballute system with perfect-gas model using effective γ=1.2 for Titan Organics Explorer.

The interacting flow simulation in Fig. 9 uses inter-block boundary communication between the spacecraft grid domain and the ballute grid domain. In this case, the flow passing into the Mach disk along the axis has already been processed through the spacecraft bow shock and wake, resulting in reduced dynamic pressure flow (less than 10% of freestream dynamic pressure at z = 10.0). A reverse flow sets up from the original location of the Mach disk towards the base of the spacecraft. At these conditions, a steady condition is achieved where the leading edge of the interaction stabilizes at a position 16 m behind the base of the spacecraft.

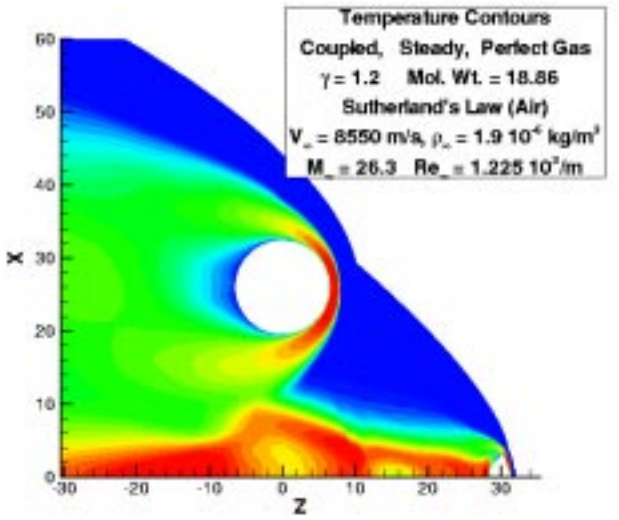

Figure 10: Temperature distribution in plane of symmetry using factor 10 increase in free stream density to 1.9 10^{-6} kg/m^3.

Recent numerical results by Hornung[5] for inviscid interacting flow between a spacecraft and ballute indicate strong unsteady interactions with waves that completely envelope the spacecraft. A steady interaction was never achieved in the inviscid model. In the present simulation (Fig. 10), an increase in the Reynolds number (through increase in freestream density) produces a much stronger interaction, enveloping the base of the spacecraft as in Hornung's inviscid simulations. However, the flow appeared to be nearly steady in the present viscous simulation; some weak, time-like oscillations were evident in the base of the

towing spacecraft though the simulation was not time-accurate.

Hot gases forced upstream in the interactions will have adverse impact on the aeroheating to the base of the spacecraft, as demonstrated in Fig. 11. Changes to heating associated with changes in density are substantially masked with the non-dimensionalization, thus highlighting the effect of the interaction. The right side of Fig. 11 shows the heating distribution around the cylindrical cross section of the ballute. The spacecraft-ballute interaction has no effect on the ballute portion of the system. The left side of Fig. 11 shows the heating distribution around the Viking shaped spacecraft. The stronger interaction at the higher density causes the dimension-less heating pattern to increase by a factor of approximately three (from values less than 0.1 to values greater than 0.3).

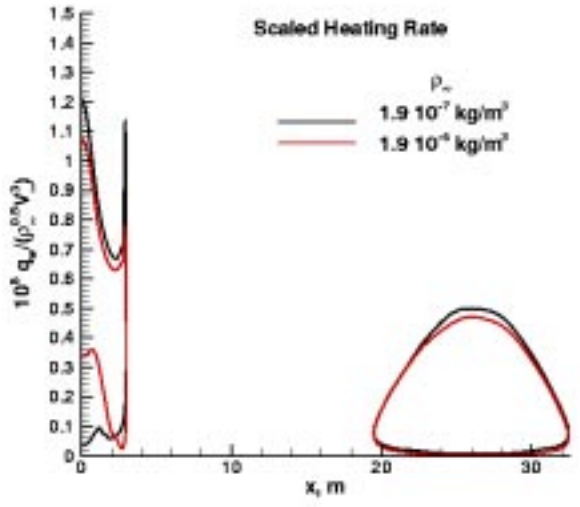

Figure 11: Heating distribution around spacecraft (left) and ballute (right) for nominal density (1.9 10^{-7} kg/m^3)

Additional thermal protection to the base of the towing spacecraft may be required for some combinations of towline length and Reynolds number in the toroid ballute system as a consequence of this backwash. Ideally, the towline should be long enough to avoid the backwash heating on the base but short enough to allow the wake to pass through the core of the toroid without choking. Still, these results add credibility to the design concept that a toroid ballute system can avoid interaction-heating effects on the flexible ballute surface itself. Future work will focus on 3D interaction effects and the possibility of using an elliptical toroid to generate lift in addition to drag.

Spacecraft – Sphere Interactions

Separation 30 m ≤ L ≤ 200 m :

Spacecraft – sphere interactions are expected to be stronger than spacecraft - toroid interactions because there is no flow-through path behind the interaction region. Consequently, a longer separation distance (longer towline) will be required. A sufficiently long separation distance, L, will avoid bow shock and wake recompression shock impingement onto the inflatable ballute surface material. Results in this section will explore aeroheating as a function of towline length in an attempt to answer how long is “sufficiently” long.

Titan Organics Explorer cases were simulated for separation distances of 30, 40, 50, 100 and 200 m. Freestream conditions and gas models are identical to the space-craft – toroid interaction cases discussed in the previous section. A spherical ballute radius of 35 m was specified.

A representative grid is presented in Fig. 12 for the 40 m separation. The towing spacecraft is resolved with 125 circumfer-ential cells and 64 cells from the body to the outer boundary. The spherical ballute domain is resolved with 56 circumferential cells and 44 cells from the body to the inflow boundary. The domain spanning the distance between the spacecraft outflow and the ballute inflow is resolved with 58 span-

wise cells and 56 cells from the axis to the farfield boundary. The number of spanwise cells will vary with separation distance to maintain approximately constant cell size. Cell Reynolds numbers at the surface are of order 1. Solutions are grid converged except in the vicinity of shock impingement on the spherical ballute, as will be described subsequently.

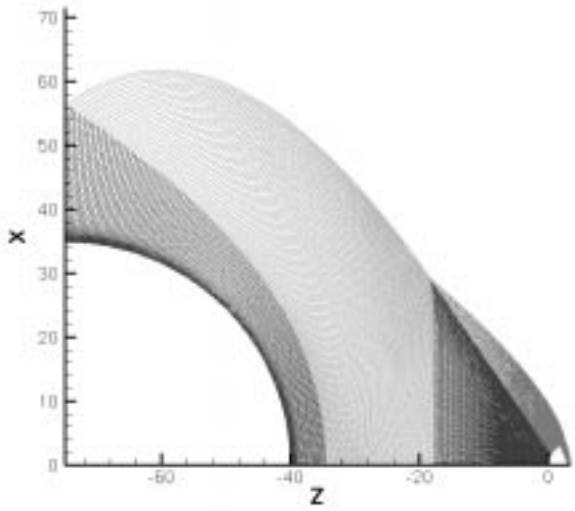

Figure 12: Mesh over spacecraft – spherical ballute system with L=40 m.

Temperature contours for a separation distance of 40 meters are featured in Fig. 13 as an example of the results acquired for different towing distances. For each tow distance, excluding the 200-meter case, reverse flow extends from the front of the sphere toward the base of the spacecraft. This recirculation is caused by interaction between low dynamic pressure flow in the wake of the towing spacecraft and the high dynamic pressure region ahead of the spacecraft bow shock. Fig. 13 shows that the recirculation leading edge is located 8 meters from the front of the sphere. Examination of the results for the other separation distances studied shows that this result is independent of tow length for lengths less than 200 meters. Grid refinement changes the result only slightly. No recirculation is present for a separation distance of 200 meters.

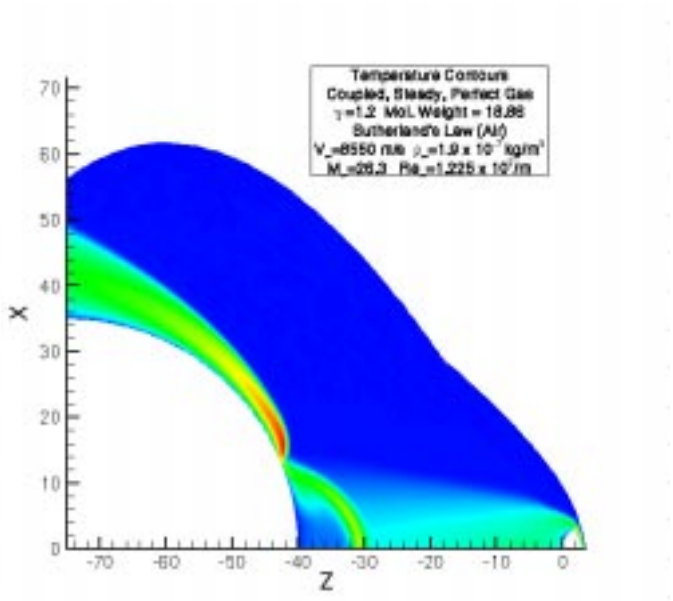

Figure 13: Temperature distribution in plane of symmetry for interacting system with L=40 m.

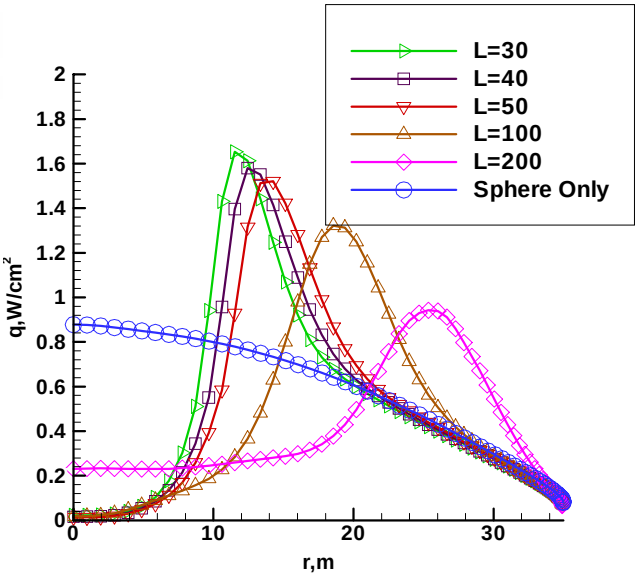

Figure 14: The effects of varying separation distances on wall heat transfer rate.

Fig. 14 shows the effect of varying separation distance on ballute wall heat transfer rate. Trends in the results for ballute surface pressure and surface

temperature as a function of separation distance are similar to those for wall heat transfer rate. To facilitate comparison, the non-interacting result for a 70-meter diameter sphere with the same free stream conditions is included in the figure. A large heating spike due to impingement of the spacecraft bow shock on the ballute is evident. (This behavior is further explored in subsequent grid convergence study.) As the separation distance is increased, the magnitude of the heating spike is decreased. Also, for $30 \leq L \leq 100$, surface heating approaches zero at the ballute geometric stagnation point. This behavior is thought to be a consequence of the strong expansion and relatively high energy-flux into the surface originating from the shock impingement zone.

Vacuum like pressures and densities are computed in the near wake of the towing spacecraft. Pressure levels are on the order of 10^{-20} N/m^2, while densities are as low as 10^{-18} kg/m^3. These low values for density are outside the limits of the continuum approximation. DSMC simulations are required to better quantify interaction effects initiated behind this near wake core.

Fig. 15 shows how the ballute drag coefficient changes with varying separation distance. Only contributions from the spherical ballute are included. The drag reaches a maximum at a tow length of 50 m. As the distance is increased, the ballute is almost completely enveloped in the low dynamic pressure flow of the spacecraft wake, resulting in reduced drag.

Results of Figs. 14 and 15 make a strong case that 200 m (33.3 spacecraft diameters, 2.86 ballute diameters) is not a "sufficiently" long towline. A shock impingement spike still exists on the flexible ballute surface and the drag effectiveness of the spherical ballute is substantially reduced because it is immersed in the low dynamic pressure of the spacecraft wake core. A simple extrapolation to longer towline distances indicates that drag effectiveness will decrease further before recovering the non-interacting sphere limit in Table 1. A simulation of longer towline distances (possibly using a space-marching approach to define wake growth) will be deferred pending further system option studies.

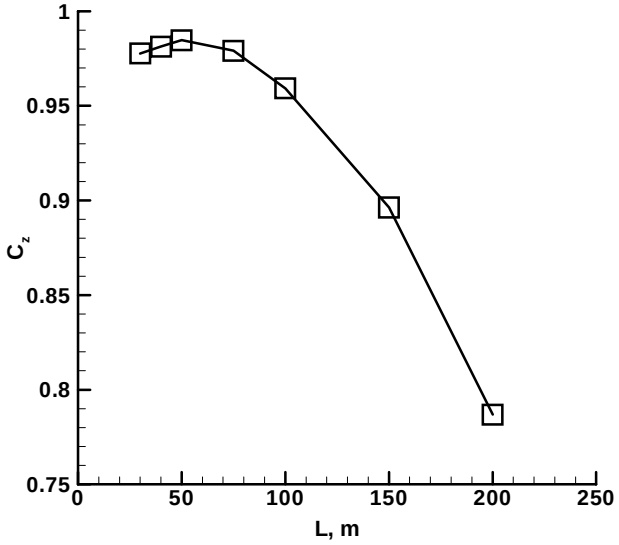

Figure 15: Effects of varying separation distance on ballute drag coefficient.

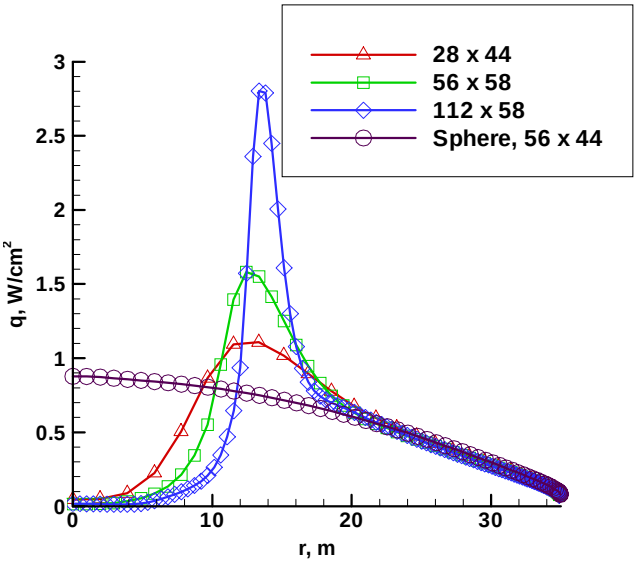

Figure 16: Results of grid convergence study on heating for a separation distance of 40 meters.

The effects of grid convergence on the heat transfer rate for a 40-meter separation distance are shown in Fig. 16. As the grid is refined (predominantly in the circumferential direction), the heating spike at the shock impingement location sharpens and increases. Grid resources are defined in Fig. 16. Note that increased circumferential resolution around the spherical ballute was matched by corresponding increase of resolution across the blocks containing the spacecraft wake core. Even on the finest grid the solution is not yet grid converged. Further refinements on this configuration were not executed because the overheating spike already indicates likely system failure.

All of the solutions for the spacecraft sphere interaction achieved steady state on the standard grid and nominal freestream conditions. A preliminary, coarse grid solution for the L=100 case exhibited unsteady motion (using a first-order time-accurate simulation) which disappeared on the finer, baseline grid. Flow was marginally unsteady at a factor 10 higher Reynolds number (factor 10 increase in freestream density) for a simulation of the L=40 test case (not shown). The upstream reverse flow extended all the way to the base of the spacecraft in this higher Reynolds number case.

In summary, for the range given by $30 \leq L \leq 200$, baseline grid trends predict shock impingement on the ballute surface that causes a local heating spike. For L=40, the grid convergence study indicates a peak heating level at impingement that probably exceed limits of lightweight, inflatable materials. The heating spike decreases with increasing L but drag effectiveness is reduced as well. More definitive conclusions and more comprehensive grid convergence studies are deferred until more appropriate simulations using DSMC (at least in the near wake core) are implemented.

Separation: L=0

The limit of L approaching 0 brings the spacecraft inside the shock layer of the ballute. Stagnation point heating on the spacecraft is reduced because the spacecraft is enveloped in the low-subsonic domain of the ballute. Consequently, the effective radius of the larger body moderates heat transfer.

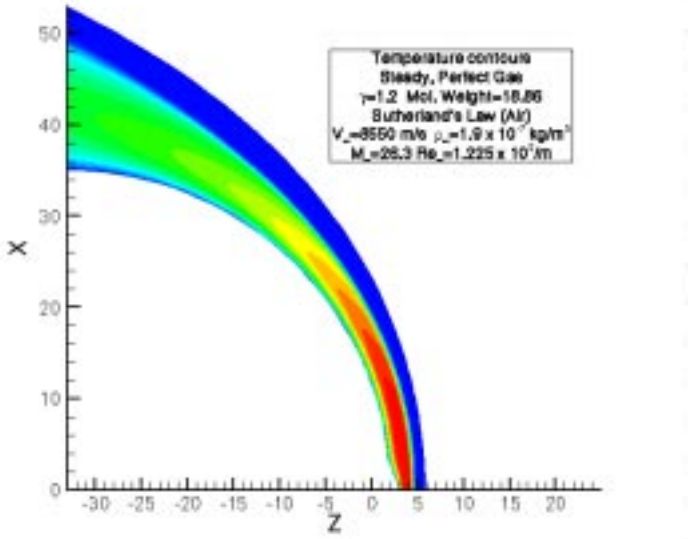

Figure 17: Global view of temperature contours in symmetry plane of clamped ballute system.

A simulation is executed in which the base of the "towing" spacecraft is depressed into the spherical ballute. This treatment simplifies the grid generation process. It also enables a system design in which the spacecraft backshell is replaced by the ballute deployment system that is clamped to the base of the spacecraft. In this approach, the ballute is unclamped from the spacecraft (rather than cutting a towline) when the appropriate ΔV_∞ is obtained.

Temperature contours in the plane of symmetry for the clamped ballute system are shown in Fig. 17. Freestream conditions are identical to those defined in the previous section. On this scale the spacecraft appears

as a small bump on the nose of the spherical ballute. The magnified view in Fig. 18 shows that the spacecraft axial dimension is approximately equal to the thermal boundary layer thickness on the ballute and only a small perturbation of the boundary layer edge is evident.

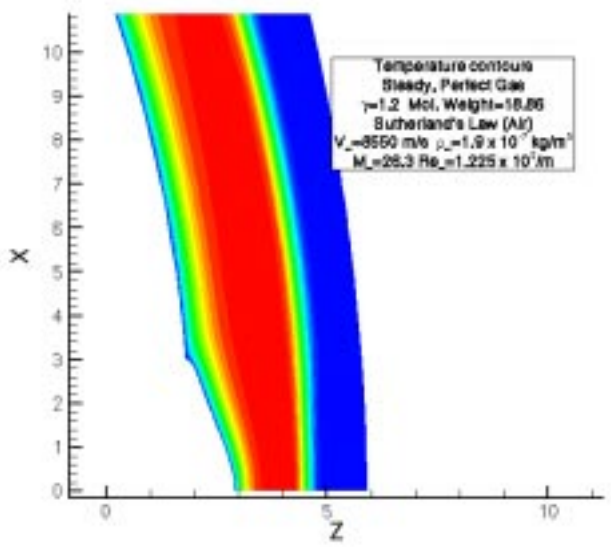

Figure 18: Detail view of temperature contours in symmetry plane of clamped ballute system.

The heat-transfer distribution for the clamped ballute system is presented in Fig. 19. The distribution for the spacecraft alone, the ballute alone, and the clamped system are compared. It is evident that the clamped system is a win-win situation for thermal protection system requirements. The clamped-system heating rate on the ballute is everywhere smaller or equal to the ballute alone values. Flow off the spacecraft shoulder onto the ballute shows no increase in heating; probably because the spacecraft shoulder radius is small relative to the boundary layer thickness. Heating on the spacecraft is reduced by about a factor of two because of the larger effective radius of the system. The heating spike over the spacecraft shoulder associated with the rapid expansion and thinning of the boundary layer is completely eliminated; there is no longer a rapid expansion off the shoulder. Finally, since the spacecraft base is essentially embedded in the ballute there is no significant aeroheating (other than thermal radiation from within the inflated ballute).

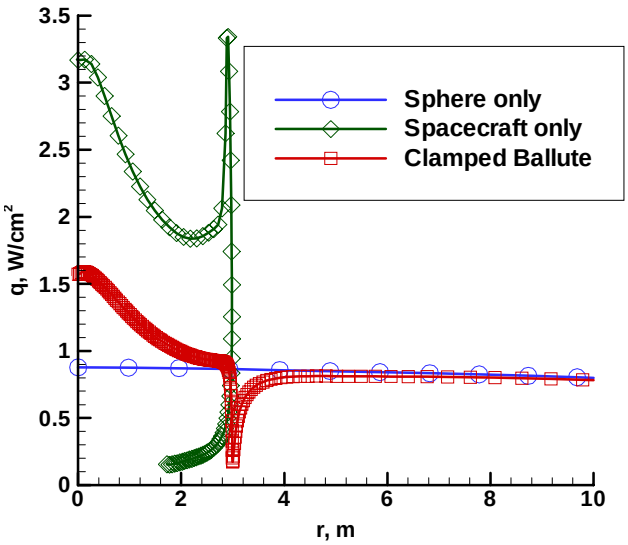

Figure 19: Heating over ballute alone, spacecraft alone, and the clamped spacecraft ballute system.

System design issues such as aerodynamic stability are currently being evaluated. Other possible design challenges not yet addressed include positioning of reaction control system jets and aerothermodynamic interference effects encountered when the spacecraft is unclamped. Nevertheless, the favorable aeroheating with reduced TPS weight, the possible elimination of a backshell and elimination of a towline and towline deployment system make the clamped ballute approach very attractive.

Concluding Remarks

Continuum flow analyses of towed and clamped ballute systems are discussed, in which the ballute is released from the

spacecraft after appropriate ΔV_∞ is obtained during a hypersonic aeropass. Non-interacting simulations on spherical and toroidal ballutes provide initial limits that establish credibility of the concept from an aeroheating perspective. Current results are presented as an interim report in an ongoing study.

Geometry parameters, gas chemistry effective γ, and Reynolds number were investigated to assess the likelihood of adverse interaction effects to aeroheating on the toroidal ballute system. Ideally, interactions are avoided if the spacecraft wake (including bow shock) passes cleanly through the hole of the toroid (and towline wake effects can be ignored). Adverse interactions are encountered in the toroidal system if significant choking occurs in the core; however, current simulations indicate that such adverse interactions can be avoided. The most significant adverse interaction appears to be a reverse flow back through the core of the spacecraft wake that may require increased thermal protection to the spacecraft base.

Interaction effects as a function of towline length were studied for spherical ballute systems comprised of a 3 m radius spacecraft and a 35 m radius ballute. Separation distances from 30 to 200 m were included in the study. At these tow distances, the spherical ballute encounters a shock impingement that leads to unacceptably high localized heating and/or compromised drag effectiveness as the ballute encounters reduced dynamic pressure in the spacecraft wake. Longer towline distances ($L > 200$ m) have not yet been tested. Concern remains that requisite towline length is so long that mass of the towline and its deployment system will preclude this design option.

In both the toroidal and spherical simulations, regions of high Knudsen number in the spacecraft wake were computed in which the continuum, Navier-Stokes simulations are compromised. As system concepts are refined, it is planned to revisit these simulations with a coupled DSMC and continuum analysis.

Finally, a very positive variation of the towed spherical ballute system employs a zero towline length (clamped system). In this design the spacecraft is contained fully within the low subsonic shock layer of the ballute and is nearly engulfed within the ballute boundary layer. Heating to the spacecraft forebody is reduced by a factor of two or greater (for the particular system considered here) and no adverse aeroheating is induced on the ballute. Towlines and associated deployment systems are obviated in this design concept. Spacecraft aft heatshield mass requirements may also be substantially reduced. Aerodynamic stability and possible adverse interactions on separation (unclamping) have not yet been evaluated for this concept.

References

[1] Hall, J. L.: "A Review of Ballute Technology for Planetary Aerocapture", Presented at the 4th IAA Conference on Low Cost Planetary Missions, Laurel, MD, May 2-5, 2000.

[2] Hall, Jeffery L.; and Le, Andrew K.: "Aerocapture Trajectories for Spacecraft with Large Towed Ballutes," Paper AAS 01-235, Feb 2001

[3] Gnoffo, Peter A.: "Computational Aerothermodynamics in Aeroassist Applications," AIAA 2001-2632, June 2001.

[4] Gnoffo, Peter A.; Gupta, Roop N.: and Shinn, Judy L.: "Conservation Equations and Physical models for Hypersonic Air Flows in Thermal and Chemical Nonequilibrium," NASA TP-2867, 1989.

[5] Hornung, H. G.: "Hypersonic Flow Over Bodies in Tandem and Its Relevance to Ballute Design" AIAA 2001-2776, June 2001. http://www.galcit.caltech.edu/~hans/ballute/ring2.mpg